Chemical Science

ROYAL SOCIETY OF CHEMISTRY

EDGE ARTICLE

View Article Online
View Journal | View Issue

Cite this: *Chem. Sci.*, 2022, **13**, 9921

All publication charges for this article have been paid for by the Royal Society of Chemistry

Received 10th May 2022
Accepted 2nd August 2022

DOI: 10.1039/d2sc02597c

rsc.li/chemical-science

Ferroptosis promotes sonodynamic therapy: a platinum(II)–indocyanine sonosensitizer†

Yidan Lai,‡ Nong Lu,‡ Ai Ouyang,‡ Qianling Zhang and Pingyu Zhang *

Sonodynamic therapy (SDT) has unique advantages in deep tumour ablation due to its deep penetration depth, showing great preclinical and clinical potential. Herein, a platinum(II)–cyanine complex has been designed to investigate its potential as a SDT anticancer agent. It generates singlet oxygen ($^1O_2$) under ultrasound (US) irradiation or light irradiation, and exhibits US-cytotoxicity in breast cancer 4T1 cells but with negligible dark-cytotoxicity. Mechanistic investigations reveal that **Pt-Cy** reduces the cellular GSH and GPX4, and triggers cancer cell ferroptosis under US irradiation. The metabolomics analysis illustrates that **Pt-Cy** upon US treatment significantly dysregulates glutathione metabolism, and finally induces ferroptosis. *In vivo* studies further demonstrate that **Pt-Cy** inhibits tumor growth under US irradiation and its efficiency for SDT is better than that for PDT *in vivo*. This is the first example of platinum(II) complexes for sonodynamic therapy. This work extends the biological applications of metal complexes from PDT to SDT.

Introduction

Sonodynamic therapy (SDT) is a new non-invasive treatment strategy.[1–4] It uses ultrasound (US) to trigger the sensitizer to produce reactive oxygen species (ROS) to kill cancer cells.[5–7] Compared with light, US shows deeper tissue permeability, which has great advantages in the treatment of deep tumours.[8,9] However, so far, the mechanism of ROS generation by SDT is not clear; one of the most representative and reasonable mechanisms is called "sonoluminescence". This mechanism indicates that light will be generated during the irradiation of the solution with US. This light can further stimulate the acoustic sensitizer to generate electron–hole (e–h^+) pairs, and finally achieve the effect of ROS generation in a water environment.[10] The sonosensitization efficiencies and ROS quantum yields are essential prerequisites for SDT.[11,12] Therefore, designing and developing excellent sonosensitizers is a crucial topic in the development of SDT. Recently, many nano-sonosensitizers showed superior physiochemical properties,[4] but the clinical translation remained unresolved because of non-biodegradation and uncertain composition. In contrast, small molecule sonosensitizers have the advantages of clear structure and easy metabolism, which are conducive to clinical applications.[10]

The development of platinum-based anticancer drugs, including cisplatin, carboplatin and oxaliplatin, represents one of the great successes in the field of metals in medicine.[13] However, their use can be accompanied by side effects and drug resistance.[14] In order to overcome these limitations, platinum(IV) prodrugs activated by reduction or light induction have achieved promising therapeutic effects in the past few decades.[13,15] Recent work aimed to study phosphorescent Pt(II)-based photosensitizers (PSs) for PDT,[16–21] which may have lower side effects and different mechanisms of action to avoid resistance to platinum chemotherapeutic drugs.

Continuous efforts have been made to overcome the light limitations associated with PDT through the development of near-infrared light (NIR)[22] or two-photon (TP) light irradiation-based PSs.[23,24] However, the problem of limited penetration into tumor sites has not yet been solved.[25] In contrast, US can reach deep organs. Moreover, US has been used for clinical diagnosis in hospitals, and thus SDT may be a promising cancer treatment strategy because of its non-invasiveness and cost-effectiveness.

Based on the above background, we designed and synthesized a platinum(II) complex conjugating a cyanine framework (**Pt-Cy**) (Fig. 1a), and investigated its SDT effect. The results showed that the **Pt-Cy** could generate ROS under US or light irradiation, and exhibited US-induced cytotoxicity towards breast cancer 4T1 cells (IC_{50} = 6.94 μM under US irradiation) but with negligible dark-toxicity. The mechanism of cell death was further investigated, and was found to display the ferroptosis characteristics of intracellular GSH content reduction, lipid peroxidation (LPO) accumulation and GPX4 down regulation. Correspondingly, the disruption of glutathione metabolism had been proved though metabolomics analysis. Finally,

College of Chemistry and Environmental Engineering, Shenzhen University, Shenzhen, 518060, P. R. China. E-mail: p.zhang6@szu.edu.cn; zhql@szu.edu.cn

† Electronic supplementary information (ESI) available: Additional spectroscopic and imaging data. See https://doi.org/10.1039/d2sc02597c

‡ These authors contributed equally.

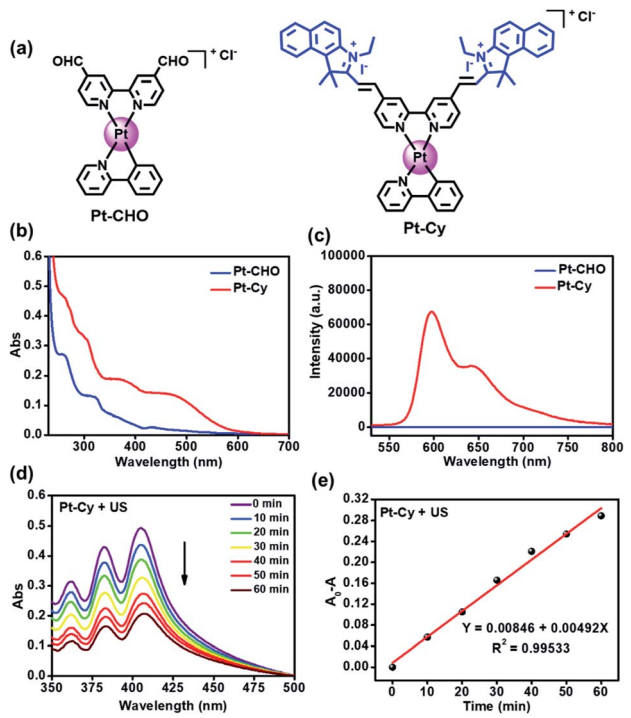

Fig. 1 (a) The chemical structures of **Pt-CHO** and **Pt-Cy**. (b) The UV-Vis absorption spectra and (c) the emission spectra of the platinum(II) complexes (10 μM) in H_2O (1% DMSO). (d) Time-dependent oxidation of DPA indicating $^1O_2$ generation by **Pt-Cy** (10 μM) under US irradiation (0.3 W cm^{-2}, 3 MHz). (e) Rate constant for DPA decomposition at 378 nm in (d).

in vivo studies demonstrated that the SDT of **Pt-Cy** showed superior potency to that of PDT.

Results and discussion

Synthesis and characterization

The synthesis of **Pt-Cy** is described in the ESI and Scheme S1.† **Pt-Cy** was fully characterized using ^{1}H NMR, ^{13}C NMR and ESI-MS spectroscopy and elemental analysis (Fig. S1–S5†). Next we studied its UV-Vis absorption and emission spectra. As shown in Fig. 1b, **Pt-Cy** exhibited obvious absorption at 400–500 nm and bathochromic-shift compared to **Pt-CHO** in UV-Vis absorption. In addition, **Pt-Cy** showed stronger red luminescence in the range from 550 to 750 nm than **Pt-CHO** (Fig. 1c). These phenomena were mainly due to the coupling of the cyanine framework in the platinum complex. Furthermore, the fluorescence lifetimes of **Pt-Cy** and the cyanine ligand (Cy) were examined. As shown in Fig. S6 and Table S1,† the average lifetime ($\tau_{Av,I}$) of Cy in DCM was 2.84 ns. After conjugating to the platinum(II) complex, the average lifetime ($\tau_{Av,I}$) of **Pt-Cy** in DCM was raised to 3.35 ns. Besides, **Pt-Cy** was stable in 1640 cell culture medium (containing 10% FBS) for 48 h (Fig. S7†).

$^1O_2$ generation

We first measured the production of $^1O_2$ using 9,10-diphenanthraquinone (DPA), which can be oxidized to 9,10-diphenanthraquinone dioxide (DPO_2) by $^1O_2$, thereby reducing its UV-Vis absorption.[26] As shown in Fig. 1d and S8,† with the increase of light/US irradiation time, the characteristic absorption peak of DPA around 378 nm decreased gradually in the presence of **Pt-Cy**. The rate constant for DPA oxidation in the presence of **Pt-Cy** and US irradiation was 0.00492 min^{-1}, which was slightly higher than the rate constant under light irradiation (0.00368 min^{-1}). Compared with the common sonosensitizer hematoporphyrin (HP) (Fig. S9†), **Pt-Cy** exhibited comparable ability to generate $^1O_2$ under US irradiation, in which the DPA oxidation rate constant of HP under US irradiation (0.00401 min^{-1}) was slightly smaller than that of **Pt-Cy**. However, HP was not stable under US irradiation (Fig. S10†). We also used 2,2,6,6-tetramethylpiperidine (TEMP) to measure $^1O_2$ generation by ESR. As shown in Fig. S11,† a three-line signal with the intensity of 1 : 1 : 1 between 3480 and 3530 G was observed in the **Pt-Cy** and TEMP mixing solution under light irradiation or US irradiation. Furthermore, 5,5-dimethyl-1-pyrroline-*N*-oxide (DMPO) was used as a $^{\cdot}$OH scavenger. As shown in Fig. S12,† neither light irradiation nor US irradiation could induce the signal of $^{\cdot}$OH in the presence of DMPO and **Pt-Cy**. $^{\cdot}$OH was also measured using methylene blue (MB),[6] which was utilized to track and capture the $^{\cdot}$OH generation during the irradiation process. As shown in Fig. S13,† the absorption peak of MB did not change with the increase of US or light irradiation time. These results showed that $^1O_2$ but not $^{\cdot}$OH was generated by **Pt-Cy** under US or light irradiation.

In vitro sonodynamic efficiency

Encouraged by the high efficiency of $^1O_2$ generation upon irradiation, we further investigated **Pt-Cy** for SDT and PDT in 4T1 mouse breast cancer cells. First, the subcellular distribution of **Pt-Cy** in the living 4T1 cells using inductively coupled plasma mass spectrometry (ICP-MS) analysis was studied. As shown in Fig. S14,† the mitochondria were found to contain a significantly high quantity of platinum compared to the lysosomes and nucleus. Our previous work had proven that the appropriate and safe US irradiation power was 0.3 W cm^{-2} and the irradiation time was 20 min.[8] Herein, US irradiation of 20 min with a power of 0.3 W cm^{-2} also was selected in the following experiments. The parameters of US used in this work are listed in Table S2.† As shown in Fig. 2a, all cell viabilities of each concentration group of **Pt-Cy** alone were higher than 75% without irradiation, suggesting its low dark cytotoxicity. However, after US irradiation, **Pt-Cy** was highly sono-toxic towards 4T1 cells and the IC_{50}(US) value was 6.94 μM. Under light irradiation, **Pt-Cy** was also photo-toxic and its IC_{50}(light) value was 15.01 μM (Fig. 2b), which was slightly higher than that under US irradiation. Observing in the bright field, cells treated with increasing concentration of **Pt-Cy** under US irradiation lost their original shapes and died, illustrating the therapeutic effect of SDT (Fig. S15†). The above results showed that **Pt-Cy** had great potential for SDT.

Then 4T1 cells of six groups (control, **Pt-Cy** alone, US irradiation alone, light ($h\nu$) irradiation alone, **Pt-Cy** + $h\nu$, and **Pt-Cy** + US) were co-stained with calcein acetoxymethyl ester (calcein-AM) and propidium iodide (PI) to differentiate between live

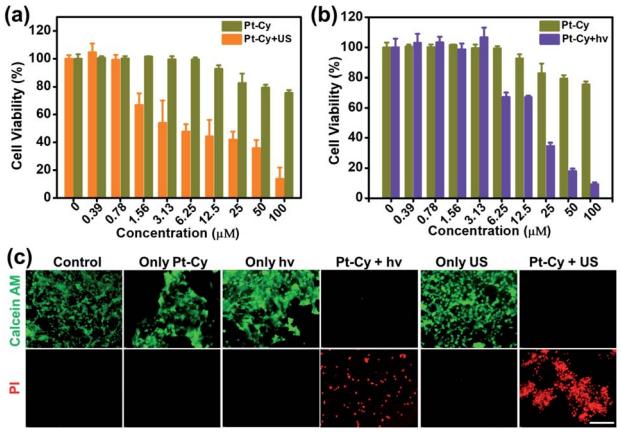

Fig. 2 The cell viabilities of 4T1 cells treated with different concentrations of **Pt-Cy** under (a) US irradiation (3.0 MHz, 0.3 mW cm^{-2}, 20 min) and (b) 465 nm light irradiation (10 mW cm^{-2}, 30 min). (c) Confocal microscopy images of the 4T1 cells treated with **Pt-Cy** (20 μM, 1 h) and then co-stained with calcein AM (4 μM, 0.5 h) and PI (6 μM, 0.5 h) after different treatments. Calcein AM: $\lambda_{ex} = 458$ nm, $\lambda_{em} = 540 \pm 30$ nm; PI: $\lambda_{ex} = 540$ nm, $\lambda_{em} = 610 \pm 30$ nm; scale bar: 100 μm.

(green color) and dead (red color) cells. As shown in Fig. 2c, the control, **Pt-Cy** alone, US irradiation alone, and light irradiation alone groups showed no red fluorescence (dead cells) but strong green fluorescence (live cells), demonstrating that 4T1 cells maintained good physiological activity in these four groups. In contrast, the **Pt-Cy** + *hν* or **Pt-Cy** + US group showed weak green fluorescence and strong red fluorescence, illustrating lots of dead cells. The results are in good agreement with the results of cytotoxicity.

In addition, we studied the ability of **Pt-Cy** to produce $^1O_2$ in 4T1 cells under light or US irradiation. Singlet oxygen sensor green (SOSG) was used as a probe to monitor the production of $^1O_2$.[8] Confocal microscopy showed that the fluorescence of 4T1 cells incubated with **Pt-Cy** and SOSG after US/*hν* treatment was much stronger than that of the control group (Fig. S16†), indicating that **Pt-Cy** produced $^1O_2$ after irradiation. The fluorescence signal of the **Pt-Cy** and US/*hν* treated group was decreased in the presence of NaN_3 (a $^1O_2$ scavenger). We further performed the DCFH-DA assay in 4T1 cells (Fig. S17†). The fluorescence intensity of 4T1 cells treated with **Pt-Cy** + US/*hν* treatment was stronger than that of the control group. The results suggested that lots of intracellular $^1O_2$ was produced by **Pt-Cy** under irradiation which then killed cancer cells.

Ferroptosis mechanism

Subsequently, the mechanism of **Pt-Cy** leading to tumor cell death under US irradiation was studied. Mass production of ROS can disturb the oxidative balance of cells, while the failure of GSH-mediated scavenging of lipid peroxides (LPO) affected by oxidative stress will activate ferroptosis.[27] Thus we first detected the ability of **Pt-Cy** to degrade GSH in solution. As shown in Fig. 3a, with the increase of US irradiation time, the absorbance of GSH in the mixed solution at 412 nm decreased, indicating that the content of GSH decreased gradually and transferred to GSSG in the presence of **Pt-Cy**. As shown in the

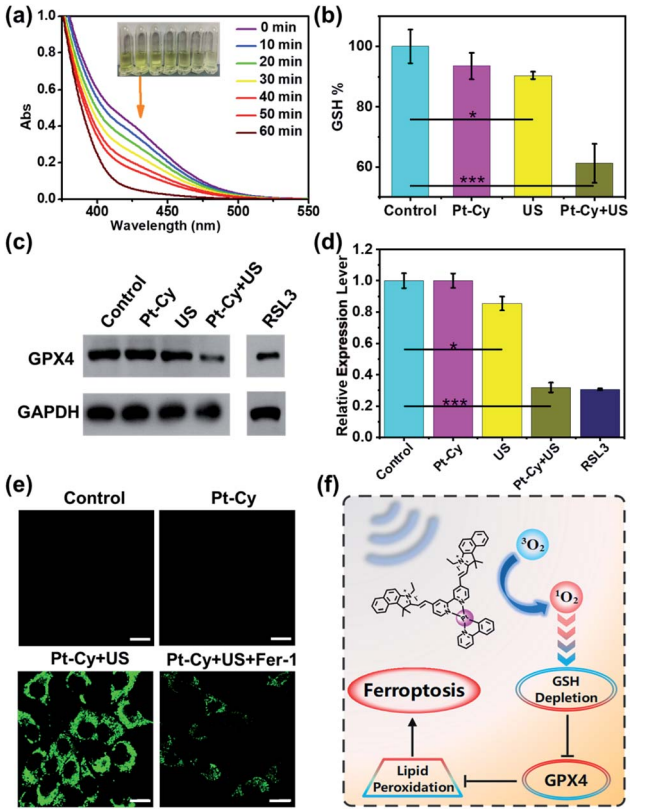

Fig. 3 Mechanism of ferroptosis. (a) Time-dependent GSH depletion by **Pt-Cy** upon US irradiation for 60 min. (b) The GSH levels in 4T1 cells after different treatments. Statistical significance was calculated with two-tailed Student's *t*-test (*$p < 0.05$, **$p \leq 0.01$ or ***$p \leq 0.001$). (c) Western blot analysis of GPX4 in 4T1 cells after different treatments. (d) The relative expression levels of GPX4 were calculated from (c). Statistical significance was calculated with two-tailed Student's *t*-test (*$p < 0.05$, **$p \leq 0.01$ or ***$p \leq 0.001$). (e) The fluorescence images of lipid peroxides in C11-BODIPY stained 4T1 cells after different treatments. C11-BODIPY: $\lambda_{ex} = 488$ nm; $\lambda_{em} = 570 \pm 50$ nm; scale bar: 20 μm; US irradiation: 3.0 MHz, 0.3 mW cm^{-2}, 20 min. (f) The mechanism of ferroptosis in the SDT process.

graphs, the color of the mixed solution became shallower and shallower. We further detected the GSH levels in the cells, and found that the GSH level in the **Pt-Cy** + US group was significantly lower than that in the other three groups (control, **Pt-Cy** alone, and US alone) (Fig. 3b). It can be concluded that **Pt-Cy** can induce the degradation of GSH levels in cells under US irradiation.

GSH acts as a cofactor in the detoxification of GPX4 catalyzed lipid peroxides to lipid alcohols. GSH intake can induce ferroptosis through circuitous inhibition of GPX4.[28–30] Thus we measured the GPX4 expression in cells by western blot assay. RSL3, as a positive control, is a known substance that can induce ferroptosis. As shown in Fig. 3c and d, **Pt-Cy** did not reduce GPX4 expression of the cells without US irradiation. However, under US irradiation, **Pt-Cy** significantly reduced GPX4 expression in the 4T1 cancer cells. The US irradiation alone group did not inhibit the expression of GPX4.

The lipid peroxides in cancer cells were measured using a C11-BODIPY probe[31,32] and observed using a laser confocal microscope.

Pt-Cy was incubated with 4T1 cells for 1 h, exposed to US for 20 min, and then incubated with 5 μM C11-BODIPY. As shown in Fig. 3e, C11-BODIPY in the **Pt-Cy** + US group emitted bright green fluorescence, and the fluorescence intensity was much higher than that in the group exposed to dark conditions. Ferrostatin-1 (Fer-1) can inhibit lipid peroxidation and the death of iron-dependent cancer cells.[33] Our experiment found that the Fer-1 pretreated group can effectively decrease the fluorescence intensity. Therefore, the mechanism of tumor cell death caused by **Pt-Cy** probably be ferroptosis. Therefore, the $^1O_2$ generation for SDT can effectively consume GSH, inhibit the level of GPX4 and cause lipid peroxides and finally induce ferroptosis (Fig. 3f).

Metabolomics analysis

The rapid development of untargeted metabolomics has paved the way for analyzing the metabolic features in cancer cells and achieving deeper understanding of mechanisms in cancer therapy.[34,35] To explore the molecular mechanism of **Pt-Cy** against 4T1 cells upon US irradiation, we further assessed the metabolomic profiles of 4T1 cells in the control, US, **Pt-Cy** and **Pt-Cy** + US groups using the ultra-performance liquid chromatography tandem mass spectrometry (UPLC-MS/MS) method. As shown in the principal components analysis (PCA) score plot (Fig. 4a and S18a†), each group showed a good separation trend in both positive and negative ion modes. Through screening (fold change < 0.67/>1.5 and p-value < 0.05), between the control and **Pt-Cy** + US groups, 115 metabolites were identified with significant differences in positive ion mode (Fig. 4b and Table S3†), while the negative ion mode had 47 differential metabolites (Fig. S18b and Table S4†). The above differential metabolites were imported into the MetaboAnalyst website for further pathway analysis. The results revealed that the most altered metabolites in both positive and negative ion modes between the control and **Pt-Cy** + US groups were mainly involved in purine metabolism and glutathione metabolism (Fig. 4c and S19†). The heat maps of differential metabolites in each treatment group are shown in Fig. 4d and S18c.† Notably, L-glutamate (*ca.* 28.44-fold), spermidine (*ca.* 11.55-fold), GSSG (*ca.* 10.29-fold), 5-oxoproline (*ca.* 9.48-fold), gamma-glutamylcysteine (*ca.* 9.09-fold) and NADP (*ca.* 8.52-fold) intermediates involved in glutathione metabolism, were dramatically upregulated following the **Pt-Cy** + US treatment compared to the control groups. However, 5-oxoproline, L-glutamate and gamma-glutamylcysteine were key substances participating in GSH synthesis. The accumulation of GSSG, which generally reduced to GSH with the help of nicotinamide adenine dinucleotide phosphate (NADPH), was potentially toxic to cells.[36] In addition, it was reported that the elevation of purine metabolism triggered the overproduction of ROS.[37,38] The metabolomics results suggested that treatment of **Pt-Cy** under US irradiation specifically disturbed the process of glutathione metabolism, and finally induced ferroptosis in 4T1 cells.

In vivo sonodynamic therapy

Based on the *in vitro* results, we further studied the feasibility of using **Pt-Cy** to inhibit tumor growth *in vivo* under US irradiation

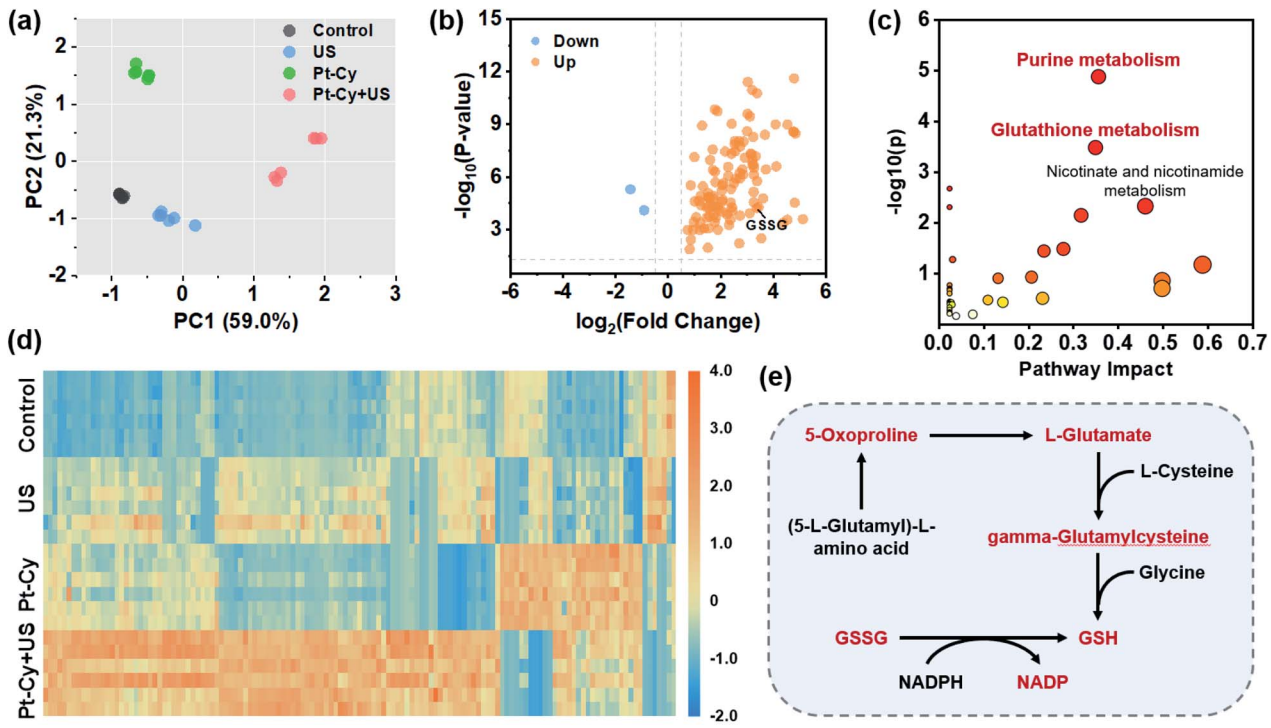

Fig. 4 Metabolomics analysis. (a) PCA score plot showing differences between the control, US, **Pt-Cy** and **Pt-Cy** + US groups of 4T1 cells. (b) Volcano plot demonstrating altered metabolite levels between the control and **Pt-Cy** + US groups. (c) Pathway analysis of significant differential metabolites between the control and **Pt-Cy** + US groups. (d) Heat map of metabolites in each treatment group. (e) Schematic illustration of glutathione metabolism pathways. US irradiation: 3.0 MHz, 0.3 mW cm^{-2}, 20 min. Ion mode: positive.

or light irradiation. Since **Pt-Cy** is a small molecule with no specific target group, meanwhile, the results of biodistribution assay indicated that **Pt-Cy** did not accumulate at the tumor site after i.v. injection (Fig. S20†), we chose i.t. injection for *in vivo* experiments. 4T1 tumor bearing mice were randomly divided into 6 groups (5 mice in each group): (1) untreated control; (2) **Pt-Cy** alone (i.t. injection 25 μL, 500 μM); (3) US alone (3.0 MHz, 0.3 W cm^{-2}, 20 min); (4) light alone (465 nm, 10 mW cm^{-2}, 30 min); (5) **Pt-Cy** + *hν*; (6) **Pt-Cy** + US. **Pt-Cy** was injected into the tumor and the tumor was immediately irradiated with US/light (Fig. S21†). After that, the tumor was monitored using a digital caliper every 2 days up to 14 days, and the tumor volumes were calculated. As shown in Fig. 5a and b, the growth of tumors in mice treated with **Pt-Cy** + US was obviously suppressed compared to the other five groups. At the end of the experiment, all tumors were removed from the mice on day 14 and collected for photographing and weighing (Fig. 5c and d). It can be seen from the results that the average tumor weight of the **Pt-Cy** + US group was the least in all groups. Hematoxylin eosin (H & E) staining and TUNEL staining images further showed the destruction of tumor tissue in each group (Fig. 5e). There was no necrosis in the control, US alone, *hν* alone, **Pt-Cy** alone, and **Pt-Cy** + *hν* groups. By contrast, a large number of cell apoptosis and necrosis were observed in the **Pt-Cy** + US group. All *in vivo* results showed that the effect of **Pt-Cy** for SDT was better than that for PDT.

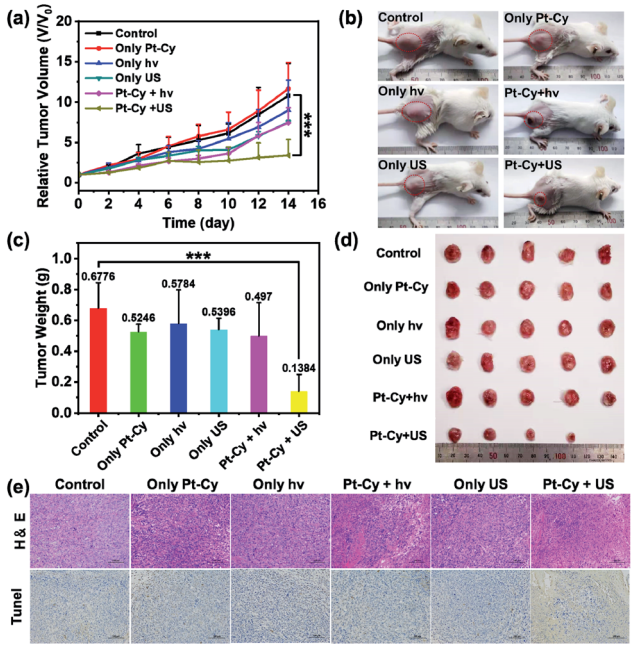

Fig. 5 *In vivo* sonodynamic therapy. (a) 4T1 tumor growth curves of mice after various treatments. Statistical significance was calculated with two-tailed Student's *t*-test (*$p < 0.05$, **$p \leq 0.01$ or ***$p \leq 0.001$). (b) Representative images of mice at day 14 after various treatments. (c) Average tumor weights of mice at day 14 post various treatments. Statistical significance was calculated with two-tailed Student's *t*-test (*$p < 0.05$, **$p \leq 0.01$ or ***$p \leq 0.001$). (d) Photos of tumors were collected from mice at day 14 after various treatments. (e) The microscopy images of H&E and TUNEL stained tumor slices, which were collected from mice at 24 h post various treatments.

Undoubtedly, when tissues are irradiated with short-wavelength light ($\lambda = 465$ nm), photons are absorbed and scattered by cells and proteins, resulting in the limited epidermal treatment.[39] US, which has already been used in hospitals for clinical diagnosis, can reach deep-seated regions and address the limitations of PDT. Thus we speculate that the limited light penetration depth is an important factor for ineffective PDT of **Pt-Cy**. However US can reach deeper tissue layers and stimulate the sonosensitizer, thus achieving excellent therapeutic effect.

Apart from the *in vivo* therapeutic effect, we also evaluated the hemocompatibility of **Pt-Cy** by hemolysis experiments to evaluate the biological safety of **Pt-Cy**. As shown in Fig. S22,† the hemolysis ratio was lower than the acceptable value (10%) even though incubated with 50 μM of **Pt-Cy**, showing good hemocompatibility and certain potential for *in vivo* application. Moreover, the H&E staining results indicated that there was no obvious tissue damage after i.v. injecting **Pt-Cy** (1.99 mg kg^{-1}) to healthy Balb/c mice (Fig. S23†). These results showed that **Pt-Cy** had good biosafety and biocompatibility.

Conclusions

In summary, we developed a novel platinum(II) complex containing a cyanine framework (**Pt-Cy**), and investigated its sonodynamic therapy. *In vitro* experiments showed that **Pt-Cy** can produce ROS under both US and light irradiation, and showed US- and photo-cytotoxicity under irradiation compared to dark conditions. Interestingly, **Pt-Cy** can significantly reduce the GSH content in cells under US irradiation, thereby leading to the accumulation of lipid peroxides and ultimately inducing ferroptosis. In addition, the metabolomics results also provided evidence that **Pt-Cy** disrupted GSH metabolism to induce ferroptosis upon US irradiation. For the *in vivo* tumor therapy, **Pt-Cy** showed more excellent sonodynamic therapeutic effect than PDT. This work expands the biological applications of metal complexes, especially from traditional PDT to SDT.

Data availability

All relevant data are presented in the main text and ESI.† The ESI contains detailed descriptions of the experimental procedures, product characterization data, NMR spectra, MS data, stability data, ROS measurements, ESR spectra, ICP-MS data, confocal microscopy images, biodistributions, hemocompatibility, and analysis of differential metabolites.

Author contributions

Y. Lai performed the cellular experiments and metabolomics analysis of **Pt-Cy**. N. Lu did *in vivo* experiments. A. Ouyang and Q. Zhang synthesized **Pt-Cy**. P. Zhang conceived and supervised the project, and wrote the manuscript with input from all authors.

Conflicts of interest

The authors declare no conflict of interests.

Acknowledgements

We appreciate the financial support of the National Natural Science Foundation of China (NSFC, 22077085, 22177078, and 21907069), the project of the Natural Science Foundation of Guangdong Province (2019A1515011958), and the Science and Technology Foundation of Shenzhen (JCYJ20210324095200002 and JCYJ20190808153209537). We appreciate the Instrumental Analysis Centre of Shenzhen University. Balb/c mice and nude mice were purchased from Liaoning Changsheng Biotechnology Co. Ltd. This work was conducted in accordance with Animal Care and Institutional Ethical Guidelines in China. And all animal experiments were carried out with permission from the Ethical Committee of Shenzhen University (certificate number: SYXK 2014-0140).

Notes and references

1 F. Gong, L. Cheng, N. Yang, Y. Gong, Y. Ni, S. Bai, X. Wang, M. Chen, Q. Chen and Z. Liu, *Nat. Commun.*, 2020, **11**, 3712.
2 X. Wang, X. Zhong, L. Bai, J. Xu, F. Gong, Z. Dong, Z. Yang, Z. Zeng, Z. Liu and L. Cheng, *J. Am. Chem. Soc.*, 2020, **142**, 6527–6537.
3 J. Ye, Q. Fu, L. Liu, L. Chen, X. Zhang, Q. Li, Z. Li, L. Su, R. Zhu, J. Song and H. Yang, *Sci. China: Chem.*, 2021, **64**, 2218–2229.
4 C. Zhang, Y. Li, X. Ma, W. He, C. Liu and Z. Liu, *Sci. China: Chem.*, 2021, **64**, 899–914.
5 W. Yue, L. Chen, L. Yu, B. Zhou, H. Yin, W. Ren, C. Liu, L. Guo, Y. Zhang, L. Sun, K. Zhang, H. Xu and Y. Chen, *Nat. Commun.*, 2019, **10**, 2025.
6 X. Pan, L. Bai, H. Wang, Q. Wu, H. Wang, S. Liu, B. Xu, X. Shi and H. Liu, *Adv. Mater.*, 2018, **30**, 1800180.
7 F. Gong, L. Cheng, N. Yang, O. Betzer, L. Feng, Q. Zhou, Y. Li, R. Chen, R. Popovtzer and Z. Liu, *Adv. Mater.*, 2019, **31**, 1900730.
8 C. Liang, J. Xie, S. Luo, C. Huang, Q. Zhang, H. Huang and P. Zhang, *Nat. Commun.*, 2021, **12**, 5001.
9 J. Xie, C. Liang, S. Luo, Z. Pan, Y. Lai, J. He, H. Chen, Q. Ren, H. Huang, Q. Zhang and P. Zhang, *ACS Appl. Mater. Interfaces*, 2021, **13**, 27934–27944.
10 S. Son, J. H. Kim, X. Wang, C. Zhang, S. A. Yoon, J. Shin, A. Sharma, M. H. Lee, L. Cheng, J. Wu and J. S. Kim, *Chem. Soc. Rev.*, 2020, **49**, 3244–3261.
11 X. Lin, J. Song, X. Chen and H. Yang, *Angew. Chem., Int. Ed.*, 2020, **59**, 14212–14233.
12 X. Wang, X. Zhong, F. Gong, Y. Chao and L. Cheng, *Mater. Horiz.*, 2020, **7**, 2028–2046.
13 T. C. Johnstone, K. Suntharalingam and S. J. Lippard, *Chem. Rev.*, 2016, **116**, 3436–3486.
14 E. Wong and C. M. Giandomenico, *Chem. Rev.*, 1999, **99**, 2451–2466.
15 J. S. Butler and P. J. Sadler, *Curr. Opin. Chem. Biol.*, 2013, **17**, 175–188.
16 M. Obata, S. Hirohara, R. Tanaka, I. Kinoshita, K. Ohkubo, S. Fukuzumi, M. Tanihara and S. Yano, *J. Med. Chem.*, 2009, **52**, 2747–2753.
17 H. Shi, C. Imberti, H. Huang, I. Hands-Portman and P. J. Sadler, *Chem. Commun.*, 2020, **56**, 2320–2323.
18 A. Naik, R. Rubbiani, G. Gasser and B. Spingler, *Angew. Chem., Int. Ed.*, 2014, **53**, 6938–6941.
19 C. Lottner, K.-C. Bart, G. Bernhardt and H. Brunner, *J. Med. Chem.*, 2002, **45**, 2079–2089.
20 G. Yu, S. Yu, M. L. Saha, J. Zhou, T. R. Cook, B. C. Yung, J. Chen, Z. Mao, F. Zhang, Z. Zhou, Y. Liu, L. Shao, S. Wang, C. Gao, F. Huang, P. J. Stang and X. Chen, *Nat. Commun.*, 2018, **9**, 4335.
21 Y.-F. Zhong, H. Zhang, W.-T. Liu, X.-H. Zheng, Y.-W. Zhou, Q. Cao, Y. Shen, Y. Zhao, P. Z. Qin, L.-N. Ji and Z.-W. Mao, *Chem.–Eur. J.*, 2017, **23**, 16442–16446.
22 K. Mitra, C. E. Lyons and M. C. T. Hartman, *Angew. Chem., Int. Ed.*, 2018, **57**, 10263–10267.
23 Z. Zhou, J. Liu, J. Huang, W. Rees Thomas, Y. Wang, H. Wang, X. Li, H. Chao and J. Stang Peter, *Proc. Natl. Acad. Sci. U. S. A.*, 2019, **116**, 20296–20302.
24 Z. Zhou, J. Liu, W. Rees Thomas, H. Wang, X. Li, H. Chao and J. Stang Peter, *Proc. Natl. Acad. Sci. U. S. A.*, 2018, **115**, 5664–5669.
25 H. M. Kim and B. R. Cho, *Chem. Rev.*, 2015, **115**, 5014–5055.
26 K.-Y. Lu, P.-Y. Lin, E.-Y. Chuang, C.-M. Shih, T.-M. Cheng, T.-Y. Lin, H.-W. Sung and F.-L. Mi, *ACS Appl. Mater. Interfaces*, 2017, **9**, 5158–5172.
27 C. Xue, M. Li, C. Liu, Y. Li, Y. Fei, Y. Hu, K. Cai, Y. Zhao and Z. Luo, *Angew. Chem., Int. Ed.*, 2021, **60**, 8938–8947.
28 S. J. Dixon and B. R. Stockwell, *Nat. Chem. Biol.*, 2014, **10**, 9–17.
29 H. Liu, S. L. Schreiber and B. R. Stockwell, *Biochemistry*, 2018, **57**, 2059–2060.
30 S. J. Dixon and B. R. Stockwell, *Annual Review of Cancer Biology*, 2019, **3**, 35–54.
31 H. Yuan, Z. Han, Y. Chen, F. Qi, H. Fang, Z. Guo, S. Zhang and W. He, *Angew. Chem., Int. Ed.*, 2021, **60**, 8174–8181.
32 N. Lu, Z. Deng, J. Gao, C. Liang, H. Xia and P. Zhang, *Nat. Commun.*, 2022, **13**, 2245.
33 X. Meng, J. Deng, F. Liu, T. Guo, M. Liu, P. Dai, A. Fan, Z. Wang and Y. Zhao, *Nano Lett.*, 2019, **19**, 7866–7876.
34 L. Chan, X. Chen, P. Gao, J. Xie, Z. Zhang, J. Zhao and T. Chen, *ACS Nano*, 2021, **15**, 3047–3060.
35 Y. Xiao, D. Ma, Y.-S. Yang, F. Yang, J.-H. Ding, Y. Gong, L. Jiang, L.-P. Ge, S.-Y. Wu, Q. Yu, Q. Zhang, F. Bertucci, Q. Sun, X. Hu, D.-Q. Li, Z.-M. Shao and Y.-Z. Jiang, *Cell Res.*, 2022, **32**, 477–490.
36 B. Niu, K. Liao, Y. Zhou, T. Wen, G. Quan, X. Pan and C. Wu, *Biomaterials*, 2021, **277**, 121110.
37 H. Zhang, Y. Lu, Y. Liang, L. Jiang and Z. Cai, *J. Hazard. Mater.*, 2020, **392**, 122475.
38 E. E. Kelley, N. K. H. Khoo, N. J. Hundley, U. Z. Malik, B. A. Freeman and M. M. Tarpey, *Free Radical Biol. Med.*, 2010, **48**, 493–498.
39 G.-H. Lee, H. Moon, H. Kim, G. H. Lee, W. Kwon, S. Yoo, D. Myung, S. H. Yun, Z. Bao and S. K. Hahn, *Nat. Rev. Mater.*, 2020, **5**, 149–165.